Nature Communications

https://doi.org/10.1038/s41467-026-69998-6

Article in Press

Large piezoelectricity in crosslinked ferroelectric polymers

Received: 6 March 2025

Accepted: 12 February 2026

Cite this article as: Yuan, Z., Li, C., Gong, Y. *et al.* Large piezoelectricity in crosslinked ferroelectric polymers. *Nat Commun* (2026). https://doi.org/10.1038/s41467-026-69998-6

Ze Yuan, Chenyi Li, Yutie Gong, Huamin Zhou & Yang Liu

Large piezoelectricity in crosslinked ferroelectric polymers

Ze Yuan[1,2,#], Chenyi Li[1,2,#], Yutie Gong[1,2], Huamin Zhou[1,*], Yang Liu[1,2,*]
[1]State Key Laboratory of Material Processing and Die & Mould Technology, School of Materials Science and Engineering, Huazhong University of Science and Technology, Wuhan, Hubei 430074, China.
[2]Guangdong HUST Industrial Technology Research Institute, Guangdong Provincial Key Laboratory of Manufacturing Equipment Digitization, Dongguan, 523808, Guangdong, China
[#]These authors contributed equally
[*]Correspondence to: H.M.Z. (hmzhou@hust.edu.cn); Y.L. (yliu1319@hust.edu.cn)

Abstract

Ferroelectric polymers exhibit numerous advantages for flexible and wearable electromechanical applications. However, their piezoelectric coefficient d_{33} remains relatively low while most previous approaches to improve d_{33} mainly focus on intramolecular engineering. Other than using intramolecular approaches, here we describe an intermolecular crosslinking strategy to achieve markedly enhanced d_{33} of -95.0 picocoulombs per newton in crosslinked ferroelectric poly(vinylidene fluoride-*co*-trifluoroethylene) copolymers. First-principles calculations reveal that intermolecular crosslinking creates strong local conformational heterogeneity facilitating ease of bond rotation near the crosslinking sites, which leads to a flattened energy landscape, resulting in substantially improved d_{33} response. We show that crosslinking enabled by solution casting process enhances piezoelectric properties across a variety of crosslinking agents. Our work offers a facile platform for rational modulation of piezoelectricity of ferroelectric polymers, representing a crucial step towards large-scale manufacturing of lightweight, flexible, and scalable ferroelectric polymers for developing high-performance electromechanical devices.

Introduction

Piezoelectric materials exhibiting the interconversion between electrical and mechanical energies are essential to modern electronics and technology including medical, industrial, military, and other electromechanical applications[1-4]. Piezoelectricity was discovered in quartz in 1880. The breakthrough occurring in 1940s was achieved in barium titanate ($BaTiO_3$) ceramics (Ref. 5), which has paved the exploration of perovskite oxides for piezoelectric applications[4]. Moreover, through the morphotropic phase boundary (MPB) concept, tremendous advances have been seen in lead-contained compounds such as lead zirconate titanate (PZT or $Pb(Zr_{1-x}Ti_x)O_3$)[6] and relaxor-PT crystals $Pb(Zn_{1/3}Nb_{2/3})O_3$-$PbTiO_3$ (PZN-PT)[7] with exceptional piezoelectric properties. MPB refers to the transition region separated by two competing symmetries with distinct polar axes near which energetically nearly degenerate polar states are facile to be varied by applying a small stimulus, leading to largely enhanced d_{33} response[8-10]. More recently, there is an exponentially growing need for practical use of piezoelectrics which expands from traditional electromechanical devices mainly based on rigid ceramics to emerging technology including soft robotics, wearable electronics, bio-implanted devices, and flexible energy harvesters[11-16]. Consequently, lightweight, flexible, and scalable organic piezoelectrics are highly desirable especially with high piezoelectric properties.

In this context, ferroelectric polymers such as poly(vinylidene fluoride) (PVDF) and its copolymers poly(vinylidene fluoride-*co*-trifluoroethylene) (P(VDF-TrFE)) are ideal organic candidates as they are lead-free, lightweight, flexible, and easy to process into large area films and other desired shapes[17-19]. Meanwhile, they show the highest piezoelectric coefficient d_{33} among piezoelectric polymers[17-19]. However, despite the growing interest for over 50 years, their intrinsic d_{33} remains much lower than that of oxide perovskites[20-27]. Various approaches including high crystallinity[22], MPB[25], ultrahigh-field poling[26] and electrostriction[27] were developed. For instance, an appreciably improved d_{33} of -63.5 pC N^{-1} was achieved at the stereochemical-induced MPB locating at 50/50 mol% composition of P(VDF-TrFE) copolymers[25] which is over twice as large as that ($d_{33}\approx$-26.0 pC N^{-1}) of PVDF homopolymers[21].

In this work, we describe a molecular mechanism by using crosslinking to enable the rational design of ferroelectric polymers with greatly improved piezoelectric properties. Previous works engineered d_{33} mainly using intramolecular design of chain conformation[25,28]. For instance, incorporation of chiral units causes local conformational disorder[28] driving the phase transition from ordered all-*trans* to disordered helix conformation mediated by the phase coexisting or MPB region[25], within which markedly increased d_{33} is achieved. However, only weak local angular distortions (about 5^o) in helical conformation can be induced by intramolecular strategy[28] (Fig. 1a), limiting the strength of conformational heterogeneity and

thus the ability to modify the flatness of the energetic landscape. Here we report a scheme based on intermolecular crosslinking which can locally create remarkably stronger conformational inhomogeneities (about 25^{o}) near the crosslinking sites. This may induce the formation of markedly flattened energetic landscape which largely benefits piezoelectricity. Our results also overturn the previous belief that crosslinking was undesired for enhancing piezoelectric response as crosslinking is detrimental to crystallization of ferroelectric polymers[29]. Moreover, our work addresses that markedly enhanced piezoelectric response induced by crosslinking is achieved in ferroelectric polymers with nearly vanishing barriers between different crystalline chain conformations, which have not been revealed in previous studies on crosslinked PVDF[30,31] with the energetically more favorable paraelectric phase yielding a weak d_{33} of -9.4 pC N^{-1} (ref. 31). Given that crosslinking acting as a powerful tool has been widely used to improve mechanical, thermal, and chemical functionalities of fluorinated polymers[32,33], our study demonstrates crosslinking as a versatile platform for developing high-performance piezoelectric polymers for flexible and wearable applications.

Results

Improved piezoelectricity by increasing local conformational heterogeneity

We synthesized crosslinked P(VDF-TrFE) copolymers with different crosslinking densities ρ whereas the representative crosslinking agents of ethylenediamine and 1,2-diaminopropane was used (Method). We choose a modest crosslinking density acting as a leverage to tune the energetic landscape of P(VDF-TrFE) copolymers near MPB mainly because the compositionally-induced MPB is sensitive to the small change in the VDF content according to the previous work[25]. Specially, we use a moderate crosslinking density from 0% to 3% according to the narrow MPB region (49 mol%$\leqslant c_{VDF}\leqslant$55 mol%) whereas crosslinking-induced dehydrofluorination may offer a tool to tune relative VDF ratio and thus the relative stability between competing crystalline phases. The underlying scheme of crosslinking with diamines typically involves the dehydrofluorination of a fluorinated polymer followed by the Michael addition reaction and the subsequent formation of C=N double bonds enabling a bridge between two fluorinated chains (Fig. 1b)[32-34]. For crosslinking we selected three typical polymer compositions which show distinct ground-state conformations: all-*trans* (c_{VDF}=65 mol%), coexisting all-*trans* and 3/1-helix (c_{VDF}=55 mol%), and 3/1-helix (c_{VDF}=47 mol%). Our Fourier-transform infrared spectroscopy (FTIR) shows the presence of crosslinked structure in terms of the appearance of IR band located at around 1652 cm^{-1} (Fig. 1c), which was regarded as the characteristic of C=N bonds[15,34]. X-ray photoelectron spectroscopy (XPS) manifests the existence of C=N double bonds introduced by crosslinking (Fig. 1d, Supplementary Figs. S1a and S1b). Moreover, our combined XPS (Supplementary Figs. S1c and S1d) and ^{1}H nuclear magnetic resonance (NMR) data (Supplementary Fig. S2) rule out the presence of

conjugated double bonds in crosslinked P(VDF-TrFE), which is consistent with the crosslinking reaction schemes occurring in fluorinated polymers[32]. The swelling experiments (Table S1) and thermogravimetric results (Supplementary Fig. S3) also support the presence of crosslinking.

We now leverage crosslinking to modulate the energetic competition between all-*trans* and 3/1-helix conformations for the MPB composition (c_{VDF}=55 mol%). Our X-ray diffraction (XRD) data show the stabilization of 3/1-helix induced by slight crosslinking (Fig. 1e and Supplementary Fig. S4a). For instance, we observe the development of the peak at 18.9° characteristic of 3/1-helix[28] at the expense of smearing of the peak intensity locating at 19.3° indicative of all-*trans* as ρ increases. There exists a critical concentration ρ_c of 0.2% above which the density of peak identified by 3/1-helix exceeds that of all-*trans*, indicating the stabilization of helical conformation[25]. Given that ρ_c corresponds to only a modest VDF loss (Δc_{VDF}=0.2 mol%) during the crosslinking reaction[31-34] (Fig. 1b), a much narrower MPB region is anticipated driven by crosslinking (Fig. 2a) compared to previous compositionally-induced MPB[25] with a Δc_{VDF} of 6 mol%. Our results therefore imply that crosslinking may be more effective to produce strong local conformational heterogeneity making helical conformation energetically more favorable above an ultralow ρ_c. Our results also indicate that crosslinking reaction cured by small molecule crosslinkers may occur in crystalline regions of thermoplastic polymers with relatively high crystallinity leading to a dramatic change in crystalline conformation (Fig. 1e and Supplementary Fig. S5), which has not been revealed in amorphous fluoroelastomers[32,33] and/or the bulky crosslinkers[15]. The enhanced local heterogeneity degree caused by crosslinking is implied collaboratively by the growth of the IR band at 506 cm^{-1} assigned to 3/1-helix in the FTIR spectra[25,28], accompanied by the smearing of the IR band at 1287 cm^{-1} assigned to all-*trans* (Supplementary Figs. S6 and S7). Consequently, our structural results indicate that intermolecular crosslinking enabled by solution casting process may give rise to stronger local heterogeneity than previous intramolecular approach obtained by suspension polymerization[25,28], leading to rapid depression of ordered conformation and the formation of a narrow MPB region ($0 \leq \rho \leq 0.2\%$).

The existence of crosslinking-driven phase transition is supported by disappearance of ferroelectric instability (Fig. 2b and Supplementary Fig. S8a) and growth of relaxor characteristics (Fig. 2c and Supplementary Fig. S9). For instance, polarization-electric field (*P-E*) hysteresis loops evolve from typical ferroelectric type (ρ=0) into pinched type loops ($\rho > \rho_c$) indicative of relaxor phase[25], in agreement with structural results (Fig. 1e). Near ρ_c, abrupt drop in the maximum polarization, remanent polarization P_r, and coercive field E_c (Supplementary Fig. S8b-8d) is observed. Such crosslinking-driven polarization evolution behavior is also observed under other frequencies (Supplementary Figs. S10 and S11). Meanwhile, as ρ increases, the relaxor characteristics reflecting the strength of local conformational

heterogeneity in helical conformation become stronger in terms of the rapidly increasing ΔT_m (defined as the frequency-dependent shift in T_m between 1 MHz and 100 Hz) at around ρ_c which saturates at ρ=1.8% (Fig. 2c). In addition, the phase transition near the dielectric peak temperature T_m become more diffused in terms of the increased diffuseness factor γ derived from modified Curie-Weiss law (Fig. 2c and Supplementary Fig. S12) and the smearing of the endothermic peak near 60 ^oC in differential scanning calorimetry (DSC) heating scans (Supplementary Figs. S13), substantiating the order-to-disorder phase transition induced by slight crosslinking.

We show that markedly augmented d_{33} is observed at ρ=1.2% (Fig. 2d), which locates at the right side of the MPB region ($0 \leq \rho \leq 0.2\%$) characterized by disordered helical conformation with strong local conformational heterogeneity (Fig. 2a). Interestingly, our finding differs from compositionally-induced MPB in non-crosslinked P(VDF-TrFE) which displays the largest d_{33} at c_{VDF}=50 mol% occurring within the MPB region[25]. Instead, our results imply that enhancing the local conformational heterogeneity may be essential to improve d_{33} in crosslinked ferroelectric polymers. The highest d_{33} measured by the Berlincourt method (d_{33} meter) is -95.0 pC N^{-1} of ethylenediamine and -93.4 pC N^{-1} of 1,2-diaminopropane which is over twice as large as that of -40.0 pC N^{-1} without crosslinking (Supplementary Fig. S14), corresponding to approximately a 3.6-fold improvement in d_{33} compared to PVDF. The existence of enhanced d_{33} is also confirmed by using the electric field induced strain at small electric fields (below the coercive field) via the converse piezoelectric effect (Fig. 2e and Supplementary Fig. S15). At low fields below the coercive field, the polarization response is entirely dominated by the elastic stretching and reorientation of dipoles, *P-E* loops are paraelectric-like (Supplementary Fig. S15). Our results also exceed that obtained by conventional MPB approach[25] by nearly 50% (Table S2), demonstrating a promising approach for design of high-performance ferroelectric polymers. We also evaluate the mechanical stability and observe that d_{33} of freestanding crosslinked piezoelectric polymers shows nearly no degradation after undergoing 10^5 mechanical cycles (Supplementary Fig. S16), indicating long-term mechanical durability. We also observe that the elongation at break is improved considerably caused by crosslinking (Supplementary Fig. S17), suggesting improved mechanical properties. As crosslinking density increases above 1%, the interchain spacing remains nearly unchanged (Supplementary Figs. S4 and S18) which may reduce the piezoelectric sensitivity. For instance, it is found that piezoelectric voltage coefficient $|g_{33}|$ is maximized at ρ=1.8% which is followed by a decline for ρ>1.8% (Supplementary Fig. S19). This is accompanied by paraelectric behavior due to the stabilization of relaxor phase for ρ>1.8% (Fig. 2a). In this regard, the crosslinked P(VDF-TrFE) with optimized piezoelectric properties is most suitable for piezoelectric applications with high piezoelectric sensitivity. Consequently, crosslinked ferroelectric

polymers may offer promising candidates to meet the ever-increasing demand for high-performance flexible piezoelectric applications near room temperature.

Generality of large piezoelectricity from local conformational heterogeneity

We show that improved d_{33} induced by crosslinking is general to other crosslinkers (Supplementary Figs. S20-S24). Interestingly, we find that improvement in d_{33} depends sensitively on crosslinkers and crosslink density while the polymer crystallinity obtained by different crosslinkers at the same crosslinking density remains nearly the same (Supplementary Figs. S25 and S26). For instance, the $|d_{33}|$ exhibits a considerable decrease from 95.0 pC N^{-1} for ethylenediamine to 68.5 pC N^{-1} for 1,12-dodecanediamine with increasing the length of zigzag-type crosslinkers at ρ=1.2% (Fig. 2f and Supplementary Figs. S20-S24). As revealed later by our theoretical computations, crosslinkers with short length may create stronger local heterogeneity near the crosslinking sites leading to more flattened energy landscape which yields a larger d_{33}. This insight also rationalizes a weak d_{33} of 11.3 pm V^{-1} reported in P(VDF-TrFE) 55/45 mol% cured by bulky polyethylene glycol[15]. Moreover, replacement of H in crosslinkers by other groups such as CH_3 may further bring intramolecular interactions resulting in the rotation of NH_2 (Supplementary Fig. S27). For instance, our computations reveal that this may result in a considerably reduced length (2.82 Å) in 1,2-diaminopropane compared to that (3.75 Å) of ethylenediamine, which tends to favor enhanced d_{33}. Meanwhile, the concomitant steric hindrance introduced by CH_3 may impose constraint for bond rotation, which in turn limits the piezoelectric response. As a result of these two competing effects, we observe that the largest $|d_{33}|$ (93.4 pC N^{-1}) by 1,2-diaminopropane is slightly smaller than that (95.0 pC N^{-1}) by ethylenediamine (Fig. 2d and Supplementary Fig. S20), which suggests the importance of steric effect caused by incorporating bulky chemical groups. Consequently, our results elucidate the crucial role of crosslinkers in tuning d_{33} which may inspire future studies to further optimize piezoelectricity through a rich spectrum of crosslinking strategies[29,30] including diamines, bisphenols, peroxides, and high-energy irradiation.

We also evaluated d_{33} responses of other polymer compositions. We find the absence of substantially improved d_{33} in crosslinked ferroelectric polymers with either ferroelectric (i.e., P(VDF-TrFE) 65/35 mol% in Fig. 2d) or relaxor phase as the ground state (i.e., P(VDF-TrFE) 47/53 mol% in Fig. 2d). To further demonstrate the generality of crosslinking strategy, we show that markedly enhanced d_{33} is achieved in other crosslinked polymers such as P(VDF-TFE) copolymer where TFE denotes the tetrafluoroethylene. The incorporation of TFE introduces head-head-tail-tail defects which stabilizes ferroelectric all-*trans* conformation against paraelectric phase in P(VDF-TFE) copolymer[35,36]. At low defect concentration such as 5 mol%, the energetic barrier between polar and non-polar phases is relatively

small[35,36] whereas crosslinking with inherently local conformational heterogeneity may help to modify the relative energetic stability between different crystalline chain conformations. Our structural evidence explicitly confirms this picture by showing a newly formed peak at the lower 2θ=18.5° (Supplementary Fig. S28) differing from the singlet at around 2θ=19.2° in pristine P(VDF-TFE) 95/5 mol% characteristic of all-*trans* conformation[32]. We show that long-range ferroelectric instability is considerably suppressed by crosslinking, like the results obtained in crosslinked P(VDF-TrFE) 55/45 mol% (Supplementary Fig. S29). Such energetically nearly degenerate phases may benefit the d_{33}. For instance, d_{33} of crosslinked P(VDF-TFE) 95/5 mol% is -44.2 pC N^{-1} at ρ=1.8% corresponding to over 145% improvement over pristine counterpart (Supplementary Fig. S30). Moreover, as the phase transition temperature usually determines the upper limit on the operating temperature of ferroelectrics, the presence of a much higher phase transition temperature (above 140 °C, Supplementary Fig. S31) in crosslinked P(VDF-TFE) 95/5 mol% than that (about 61 °C) of crosslinked P(VDF-TrFE) 55/45 mol% is conducive to practical piezoelectric applications with a wide operating temperature range. In addition, our approach is also generally applicable to ferroelectric polymer blends where crosslinking enables markedly enhanced d_{33} response (Supplementary Figs. S32-S42). As PVDF adopts the well-defined ground state corresponding to ferroelectric all-*trans* conformation like P(VDF-TrFE) 80/20 mol%, greatly enhanced d_{33} is not achieved upon crosslinking (Supplementary Figs. S43 and S44). We therefore identify that greatly augmented d_{33} driven by crosslinking requires the presence of energetically nearly degenerate phases[25,37-39], which is generic to ferroelectric polymers crosslinked by a wide range of crosslinking agents.

Origin of local conformational heterogeneity induced by crosslinking

To provide structural insights into enhanced d_{33}, we performed electric field-dependent XRD (Figs. 3a-3c). We observe that the doublet identified by phase coexistence of all-*trans* and 3/1-helix tends to merge into a singlet at around 19.6° characteristic of all-*trans* as the electric field increases. This finding is an indication of polarization rotation stemming from electric-field-induced phase transition from helical phase to *trans*-planar phase (Fig. 1a), which occurs regardless of crosslinking. Moreover, crosslinking inhibits such phase transition requiring a much higher electric field (>200 MV m^{-1}, Fig. 3c) than non-crosslinked counterpart (about 100 MV m^{-1}). For instance, the presence of a shoulder at around 19.2° remains in crosslinked case even under 200 MV m^{-1} (Figs. 3b and 3c) owing to the existence of strong local conformational heterogeneity in contrast with the non-crosslinked XRD results (Fig. 3a). Consequently, electric field-dependent XRD results provide strong structural implications that enhanced degree of local conformational heterogeneity created by crosslinking may be vital to characterize greatly improved d_{33}.

To shed light on the origin of local conformational heterogeneity, we performed density functional theory (DFT) simulations. In the light of the conformational disorder model[28], we used $\Delta\tau$ defined as local deviations of the *gauche* torsional angles from τ=60° in the regular 3/1-helix (Fig. 1a, Supplementary Figs. S45 and S46) to account for local conformational heterogeneity. We show that the values of $\Delta\tau$ away from the crosslinking sites are about 5°-7°, which are well consistent with that (≈5°) obtained by intramolecular method[28]. Figs. 4b and 4e show that the largest angular distortion $\Delta\tau_{max}$ (>15°) is always observed close to the *gauche* angle 5 corresponding to the crosslinking sites (Figs. 4a and 4d) independent of crosslinkers. We find that short ethylenediamine (3.75 Å) generates a much larger $\Delta\tau_{max}$ of 24.6° when compared with that (15.4°) of 1,3-diaminopropane (4.98 Å) indicating stronger local inhomogeneities. Meanwhile, 1,2-diaminopropane induces strongly spatially varying $\Delta\tau$ for two crosslinked chains, compared with ethylenediamine and 1,3-diaminopropane with the absence of CH_3. These theoretical results explicitly reveal the presence of strong local conformational heterogeneity induced by intermolecular crosslinking, which has not been attainable by previously intramolecular strategy[28].

Engineering local structural heterogeneity is crucial to piezoelectric coefficients of classic perovskite relaxors[40,41]. Our combined experimental and theoretical results elucidate that higher d_{33} can be achieved by increasing the local conformational heterogeneity. To correlate the local conformational heterogeneity with piezoelectric response from a molecular perspective, here we calculated the energy gain ΔU by allowing local rotation of τ by a small angle $\Delta\varphi$ ($|\Delta\varphi|\leq10°$). We find that ΔU near the crosslinking sites (i.e., *gauche* angle 5) is much lower than that at the locations (i.e., *gauche* angle 7 and 9) away from the crosslinking sites (Figs. 4c and 4f), which explains why $\Delta\tau_{max}$ occurs near the crosslinking sites (Figs. 4b and 4e). Moreover, ethylenediamine enables a smaller rotational energy barrier near the crosslinking sites than 1,3-diaminopropane (Figs. 4c and 4f), rationalizing a larger $\Delta\tau_{max}$ (Figs. 4b and 4e), which is essential to improved d_{33} (Fig. 2f). In addition, the existence of CH_3 in 1,2-diaminopropane lowers the rotational energy barrier (ΔU<0) for the angle 5 within a small angle range $0<\Delta\varphi<4°$ while it brings a considerably bigger energetic penalty than ethylenediamine and 1,3-diaminopropane at relatively larger distortive angle $\Delta\varphi$>4° (Supplementary Figs. S47a and S47c), reconciling the steric effect by CH_3. This may lead to a smaller $\Delta\tau_{max}$ than ethylenediamine (Fig. 4b and Supplementary Fig. S47b) and thus lowered d_{33} response despite shorter interchain distance. We therefore address that the smearing of rotational energies near the crosslinking sites gives rise to enhanced local heterogeneity, which completely differs from increasing interfacial energies related to local polarization and strain discontinuity in classic perovskite relaxors[40,41]. The nearly vanishing energy barriers for local bond rotations near the crosslinking sites may further flatten the energetic landscape, which brings huge responses to a small stimulus and thus generates a remarkably improved d_{33}, compared to conventional

MPB approach[25]. The mechanistic insights at the molecular scale are unambiguously supported by experimental data, validating the computational approach, which also provide further support that crosslinking here occurs mainly in crystalline domains rather than amorphous regions in previous works[15,32,33]. Consequently, we reveal that enhancing local conformational heterogeneity introduced by interchain crosslinking may benefit piezoelectricity, bringing a viable strategy for designing ferroelectric polymers with large piezoelectricity.

Discussion

Crosslinking using the same P(VDF-TrFE) 55/45 mol% copolymer has been also conducted in previous work[15] using a bulky crosslinker. By contrast, our work uses much smaller crosslinkers which yield a completely different outcome. For instance, the presence of crosslinking reactions in the amorphous region generally excludes the structural change in crystalline region as reported in previous work[15], which is completely different from the order-to-disorder phase transition in crystalline regions observed in this work. Previous studies in this field usually use long-chain crosslinkers[15,33,34] whereas the crosslinking mainly occurs in the amorphous regions as the bulky crosslinkers are difficult to enter the crystalline regions. We used the shortest length of zigzag-type crosslinkers (ethylenediamine and 1,2-diaminopropane) to present our main results in this work. Compared with ethylenediamine, 1,2-diaminopropane may be more suitable for promising large-scale applications recalling that d_{33} obtained by ethylenediamine is only slightly higher than that obtained by 1,2-diaminopropane. This mainly arises from the safety and cost concerns by using ethylenediamine which was regarded as highly regulated chemical reagents in some regions and more costly than 1,2-diaminopropane. Indeed, our main experimental findings are also in contrast with the general outcome by amorphous crosslinking in previous works[29,30]. For instance, the occurrence of crosslinking in the amorphous region would yield reduced P_r due to decreased crystallinity while it generally would increase E_c as crosslinking simply inhibits chain/bond rotation. Our experimental results on *P*-*E* loops deviate from this common belief showing the reduction in E_c due to the stabilization of 3/1-helix conformation in crystalline region. In addition, crosslinking-induced MPB-like region is achieved intermolecularly (Fig. 2a) rather than intramolecularly in previous works[25,34], which helps to expand the MPB concept in piezoelectric polymers as MPB in polymers is achieved by intramolecular approach. Our results also indicate that crosslinking agents with small molecule sizes may enter crystalline regions leading to structural evolution according to XRD data. Other evidence also supports this result such as dramatically reduced P_r (Supplementary Fig. S8b), abruptly stronger relaxor characteristics (Fig. 2c) and unique electric field-dependent XRD behavior (Figs. 3a-3c) as these data would not occur if crosslinkers were excluded from the crystalline regions of ferroelectric polymers.

The highest d_{33} is observed in the relaxor region rather than the phase coexisting region observed in compositionally-induced MPB in P(VDF-TrFE) recalling that MPB is defined as the phase transition region where both competing local relaxor order and long-range ferroelectric order coexist with each other[25]. This is mainly attributed to the presence of strong local conformational heterogeneity introduced by crosslinking. For instance, crosslinking may yield the stabilization of the short-range relaxor phase even at an ultralow ρ_c of 0.2% according to our structural and electrical results (Figs. 1e, 2b and 2c). In this regard, VDF concentration varies slightly by only a modest decrease of 0.2 mol% due to dehydrofluorination during the crosslinking reactions. As a result, this leads to the formation of a very narrow MPB region ($0 \leqslant \rho \leqslant 0.2\%$). By contrast, breaking of delicate balance between normal ferroelectric phase and relaxor phase requires reducing the VDF content by 6 mol% according to the previous work[25]. This contrasting behavior clearly illustrates the unique feature of crosslinking in generating local conformational heterogeneity which critically correlates with enhanced piezoelectric response occurring in relaxor regime instead of the phase existence region. Compared with the result observed by the compositionally-induced MPB[25], the introduction of local conformational heterogeneity may approximately account for over 40% enhancement in d_{33} response. In addition, our field-dependent structural results indicate that the presence of strong local conformational heterogeneity delays the complete phase transition from disordered phase to ordered phase rather than facilitating such phase transition. Combined with our DFT calculations, our results therefore suggest that the ease of bond rotations caused by crosslinking occurs locally rather than collectively in response to applied field, which is mainly responsible for higher d_{33} than that obtained by conventional MPB approach[25].

We have synthesized crosslinked ferroelectric polymers delivering large d_{33} of -95.0 pC N^{-1} engineered via enhancing the local conformational heterogeneity. The markedly enhanced d_{33} is demonstrated through comprehensive piezoelectric measurements as well as scalability which remains rarely reported in the literature (Table S2). The effectiveness of this molecular scheme was demonstrated with various polymer compositions and crosslinking agents, which provides a facile platform to enable the rational synthesis of new polymers with high piezoelectric properties. Ferroelectric polymer films with large piezoelectricity are easily synthesized through solution casting method with high flexibility and good scalability (Supplementary Fig. S48). Such simple and general process unlocks the door to the mass-production of outstanding ferroelectric polymers for flexible and scalable sensor and energy applications with variable device configurations.

Methods

Materials. P(VDF-TrFE) (80/20 mol%, 65/35 mol%, 55/45 mol%, and 43/57 mol%), were purchased from Piezotech at Arkema. P(VDF-TFE) 95/5 mol% was purchased from PolyK Technologies. PVDF was purchased from Sigma-Aldrich. The crosslinking agents including ethylenediamine (M_w=60.1 g mol^{-1}), 1,2-diaminopropane (M_w=74.1 g mol^{-1}), 1,3-diaminopropane (M_w=74.1 g mol^{-1}), 1,5-diaminopentane (M_w=102.2 g mol^{-1}), 1,10-diaminodecane (M_w=172.3 g mol^{-1}), and 1,12-dodecanediamine (M_w=200.4 g mol^{-1}) were purchased from Sigma-Aldrich. All solvents including *N*,*N*-dimethylformamide, cyclohexanone, tetrahydrofuran, and dimethylsulfoxide were purchased from Sigma-Aldrich. All chemicals were used as received.

Synthesis of crosslinked polymers. The ferroelectric polymer (i.e., P(VDF-TrFE) and polymer blends) powder of 300 mg was dissolved in cyclohexanone (5 ml). The P(VDF-TFE) powder of 300 mg was dissolved in *N*,*N*-dimethylformamide (5 ml). The PVDF powder of 800 mg was dissolved in *N*,*N*-dimethylformamide (5 ml). The solution was stirred with a rate of 400 r.p.m. overnight. After that, crosslinking agent (i.e., ethylenediamine) was added into the solution and stirred overnight. The solution was cast onto glass plates, followed by annealing at 220 °C for 1 h for thermal crosslinking. This optimized thermal condition was obtained through the orthogonal experiments on d_{33} obtained by different thermal conditions, as summarized in Table S3. It was observed that high d_{33} values were generally achieved across a high-temperature range (190 °C-250 °C) where the specific condition under 220 °C for 1 h yielded the maximum $|d_{33}|$ of 93.4 pC N^{-1}. Extending the reaction time (e.g., to 4 h) or further increasing the temperature (e.g., to 250 °C) did not result in further improvements in d_{33}, indicating that the property enhancement enabled by thermal processing had reached saturation. The crosslinked polymer films were peeled off from the glass plates. The crosslinked PVDF were stretched 5 times to obtain a β-phase dominated samples. The typical thickness of synthesized polymer films is about 30 μm.

Following the reaction mechanism (Fig. 1b), the crosslinking density ρ was calculated by the relationship $\rho=2\times(n/60.10)/(m/72.1)\times100$ where n and m are the masses of ethylenediamine and P(VDF-TrFE). For other crosslinkers and polymer compositions, ρ can be obtained by changing the molecular weights of polymer and crosslinking agent. The polymer blends with different ratios consisted of 70 wt% P(VDF-TrFE) 43/57 mol% and 30 wt% P(VDF-TrFE) 65/35 mol%, 85 wt% P(VDF-TrFE) 47/53 mol% and 15 wt% P(VDF-TrFE) 65/35 mol%, respectively.

NMR. ^{1}H NMR spectroscopy was conducted by using an AscendTM 600 MHz spectrometer (Bruker). The samples were dissolved in acetonitrile-d_3.

XPS. XPS spectra were recorded with a SCIENTIFIC ESCALAB 250Xi (Thermo, USA). A monochromatized Al target was employed as the excitation source with a voltage of 12.0 kV and a current

of 6 mA. The vacuum level was maintained at 5×10^{-9} mbar. Two passes of energy were utilized, with 150 eV for the survey mode and 30 eV for the high-resolutions mode. The work function was set to 4.20 eV. Charge correction was performed by referencing the high-resolution peak of C1s, which exhibited a binding energy of 284.5 eV.

Swelling measurement. Crosslinked polymer films were dipped into different solvents including *N*,*N*-dimethylformamide, dimethylsulfoxide and tetrahydrofuran, respectively. The degree of swelling was obtained by $\Delta W=((W_f-W_i)/W_i)\times100$ where W_f and W_i correspond to the weights of crosslinked P(VDF-TrFE) before and after swelling in a solvent, respectively.

XRD. XRD measurement was performed by the diffractometer (PANalytical Empyrean) under Bragg-Brentano geometry (Cu Kα1 source with the wavelength λ=1.54 Å). For electric field-dependent XRD, polymer films with gold electrodes were prepared. Silver wires were used to connect the samples with Trek 610E amplifier. To ensure electrical insulation, a Teflon layer was introduced to separate the sample from XRD sample holder. After electric field was applied by a specifical voltage generated by the amplifier, XRD scans were performed.

FTIR. FTIR spectra were obtained by using a spectrometer (Nicolet iS50R) in the attenuated total reflectance mode. The fraction of different chain conformations was estimated by calculating the relative ratio between the integration of absorption bands of different chain conformations in FTIR spectra[32].

DSC. DSC measurement was carried out by using a Diamond DSC (PerkinElmer Instruments) with a heating rate of 10 °C min^{-1}. The crystallinity can be obtained through the calculations of melting enthalpy following the relation $X_c=\Delta H_m/[x_{VDF}\Delta H_0]$, where H_m corresponds to the melting enthalpy of the polymer, calculated by integrating the melting peak, x_{VDF} is the mass ratio of VDF in P(VDF-TrFE)[15,25], and ΔH_0 is the melting enthalpy of a 100% crystalline PVDF (ΔH_0=103.4 J g^{-1}) (ref. 23). The VDF loss due to crosslinking was considered in the calculations of the crystallinity.

DMA. The stress-strain curves of the samples were tested using the Diamond DMA (PerkinElmer Instruments).

Dielectric measurement. For electrical measurements, gold electrodes of a typical thickness of 50 nm were sputtered (Quorum Q150RS plus) on both sides of the polymer films. The temperature dependence of the dielectric response was measured using an LCR meter (E4980A, Keysight) connected to an oven with a heating rate of 1 °C min^{-1} and a frequency range from 100 Hz to 1 MHz.

The dielectric constant above T_m at the frequency of 1 MHz was analyzed by using modified Curie-Weiss law which is expressed as $(T-T_m)^\gamma/C=1/\varepsilon_r-1/\varepsilon_{max}(T=T_m)$ (γ is the relaxor diffuseness factor and C is a constant). To deduce γ, the data points in terms of $\ln(1/\varepsilon_r-1/\varepsilon_{max})$ versus $\ln(T-T_m)$ were plotted whereas the slope of the curve corresponded to the value of the diffuseness factor γ.

The dielectric spectra of crosslinked P(VDF-TrFE) was analyzed by fitting the dielectric parameters with the Vogel-Fulcher law $\ln f=\ln f_0-E_a/k_B(T_m-T_f)$ (where E_a is the activation energy and f_0 is the characteristic frequency). The typical fitting results were summarized in Supplementary Fig. S49, supporting the existence of relaxor behavior in crosslinked P(VDF-TrFE) copolymers.

Piezoelectric measurement. The piezoelectric coefficient d_{33} was measured by a quasi-static d_{33}-meter (PKD3-2000, PolyK Technologies) through the quasi-static Berlincourt method (with a dynamic force of 0.25 N at a frequency of 110 Hz under an applied static force of 0.5 N).

Electric-field-induced strain measurement was used to determine d_{33} through a laser interferometer (SIOS SP-S 120E), which is similar to previous experimental setup[21,27]. The ac electric field well below E_c was applied during the strain measurement.

Before piezoelectric measurements, the samples underwent d.c. poling (i.e., electric field of 150 MV m^{-1}, 10 min) at room temperature[18].

***P-E* loop measurement.** A modified Sawyer-Tower circuit was employed in *P-E* loops measurement whereas an electric field with the triangular waveform was applied.

DFT calculations. DFT calculations were performed using the Gaussian program package[42]. The structures include crosslinker molecules (i.e., ethylenediamine, 1,2-diaminopropane, 1,3-diaminopropane, 1,5-diaminopentane, 1,10-diaminodecane, and 1,12-dodecanediamine) and two PVDF chains crosslinked with ethylenediamine, 1,2-diaminopropane and 1,3-diaminopropane were studied in our computations. The structural optimization was carried out at B3LYP/6-311+G(d,p) level of theory[43], and the DFT-D3 method with Becke-Johnson damping function was adopted for the dispersion energy correction[44,45]. We considered simplified systems relevant to our work, which are computationally tractable. Specifically, we used PVDF chains by ignoring the contribution of chiral TrFE to address the role of crosslinking in tailoring the energetics and local inhomogeneities. In this regard, the periodic boundary condition was not necessarily imposed, and the symmetry was not constrained on our structures. Initially, two identical PVDF chains with two different chain conformations, namely 3/1-helix and all-*trans*, were crosslinked by different crosslinkers including ethylenediamine, 1,2-diaminopropane and 1,3-diaminopropane, respectively. The PVDF chain was composed of 24 C atoms, 24 F atoms and 26 H atoms whereas the terminal groups were saturated with H atoms. For the 3/1-helix chain, the *gauche* angle τ was defined as the dihedral angle of sequential backbone of C-C-C-C. The *gauche* angle τ in the initial regular 3/1-helix structure was 60°. As shown in Supplementary Fig. S45, there were totally 11 C-C-C-C dihedral angles in each chain. Considering the two different PVDF conformations, the crosslinkers (with varied crosslinking degree) and total twelve molecules were optimized.

Rigid potential energy surface (PES) scans, depicting the contribution of the local rotation of the different dihedral angles to energy gain, were performed[42]. The energy gain ΔU induced by local bond rotation was calculated by allowing a specific *gauche* angle τ to rotate by a small angle $\Delta\varphi$ while the frozen constraint was imposed on the other angles. The initial *gauche* angles τ ($\Delta\varphi$=0) corresponded to the equilibrium values obtained by the above DFT calculations. Accordingly, the energy for $\Delta\varphi$=0 was fixed to be zero as the reference. $\Delta\varphi$ was set from -10^o to 10^o in a step of 1^o. By relaxing the structure, ΔE with respect to that under $\Delta\varphi$=0 was obtained.

Data Availability

The source data for Figs. 1–4 in this work are provided in the Source Data file. Source data are provided with this paper. All data are available from the corresponding author upon request.

References

1. Shrout, T. R. & Zhang, S. J. Lead-free piezoelectric ceramics: Alternatives for PZT? *J. Electroceram.* **19**, 111-124 (2007).

2. Rödel, J. Jo, W., Seifert, K. T. P., Anton, E.-M., Granzow, T. & Damjanovic, D. Perspective on the development of lead-free piezoceramics. *J. Am. Ceram. Soc.* **92**, 1153-1177 (2009).

3. Zheng, T., Wu, J. G., Xiao, D. Q. & Zhu, J. G. Recent development in lead-free perovskite piezoelectric bulk materials. *Prog. Mater. Sci.* **98**, 552-624 (2018).

4. Trolier-McKinstry, S., Zhang, S., Bell, A. J. & Tan, X. High-performance piezoelectric crystals, ceramics, and films. *Annu. Rev. Mater. Res.* **48**, 191-217 (2018).

5. Berlincourt, D. & Jaffe, H. Elastic and piezoelectric coefficients of single-crystal barium titanate. *Phys. Rev.* **111**, 143-148 (1958).

6. Jaffe, B., Roth, R. S. & Marzullo, S. Piezoelectric properties of lead zirconate-lead titanate solid-solution ceramics. *J. Appl. Phys.* **25**, 809-810 (1954).

7. Park, S.-E. & Shrout, T. R. Ultrahigh strain and piezoelectric behavior in relaxor based ferroelectric single crystals. *J. Appl. Phys.* **82**, 1804-1811 (1997).

8. Ahart, M., Somayazulu, M., Cohen, R. E., Ganesh, P., Dera, P., Mao, H.-K., Hemley, R. J., Ren, Y., Liermann, P. & Wu, Z. Origin of morphotropic phase boundaries in ferroelectrics. *Nature* **451**, 545-548 (2008).

9. Guo, R., Cross, L. E., Park, S. E., Noheda, B., Cox, D. E. & Shirane, G. Origin of the high piezoelectric response in $PbZr_{1-x}Ti_xO_3$. *Phys. Rev. Lett.* **84**, 5423-5426 (2000).

10. Fu, H. & Cohen, R. E. Polarization rotation mechanism for ultrahigh electromechanical response in single-crystal piezoelectrics. *Nature* **403**, 281-283 (2000).

11. You, Y.-M., Liao, W.-Q., Zhao, D., Ye, H.-Y., Zhang, Y., Zhou, Q., Niu, X., Wang, J., Li, P.-F., Fu, D.-W., Wang, Z., Gao, S., Yang, K., Liu, J.-M., Li, J., Yan, Y. & Xiong, R.-G. An organic-inorganic perovskite ferroelectric with large piezoelectric response. *Science* **357**, 306-309 (2017).

12. Kim, J. S., Kim, E. H., Park, C., Kim, G., Jeong, B., Kim, K. L., Lee, S. W., Hwang, I., Han, H., Lee, S., Shim, W., Huh, J. & Park, C. Sensing and memorising liquids with polarity-interactive ferroelectric sound. *Nat. Commun.* **10**, 3575 (2019).

13. Chorsi, M. T., Curry, E. J., Chorsi, H. T., Das, R., Baroody, J., Purohit, P. K., Ilies, H. & Nguyen, T. D. Piezoelectric biomaterials for sensors and actuators. *Adv. Mater.* **31**, 1802084 (2019).

14. Liu, Y., Zhou, Y., Qin, H., Yang, T., Chen, X., Li, L., Han, Z., Wang, K., Zhang, B., Lu, W., Chen, L.-Q., Bernholc, J. & Wang, Q. Electro-thermal actuation in percolative ferroelectric polymer nanocomposites. *Nat. Mater.* **22**, 873-879 (2023).

15. Gao, L., Hu, B.-L., Wang, L., Cao, J., He, R., Zhang, F., Wang, Z., Xue, W., Yang, H. & Li, R.-W. Intrinsically elastic polymer ferroelectric by precise slight cross-linking. *Science* **381**, 540-544 (2023).

16. Zhang, H. Y., Tang,Y. Y., Gu, Z. X., Wang, P., Chen, X. G., Lv, H. P., Li, P. F., Jiang, Q., Gu, N., Ren, S. Q. & Xiong, R.-G. Biodegradable ferroelectric molecular crystal with large piezoelectric response. *Science* **383**, 1492-1498 (2024).

17. Lovinger, A. J. Ferroelectric Polymers. *Science* **220**, 1115-1121 (1983).

18. Liu, Y. & Wang, Q. Piezoelectric polymers. *Encyclopedia of Polymer Science and Technology*. 1-31 (2023).

19. Zhang, L., Li, S., Zhu, Z., Rui, G., Du, B., Chen, D., Huang, Y.-F. & Zhu, L. Recent progress on structure manipulation of poly(vinylidene fluoride)-based ferroelectric polymers for enhanced piezoelectricity and applications. *Adv. Funct. Mater.* **33**, 2301302 (2023).

20. Kawai, H. The piezoelectricity of poly (vinylidene fluoride). *Jpn. J. Appl. Phys.* **8**, 975-976 (1969).

21. Furukawa, T. & Seo, N. Electrostriction as the origin of piezoelectricity in ferroelectric polymers. *Jpn. J. Appl. Phys.* **29**, 675-680 (1990).

22. Omote, K., Ohigashi, H. & Koga, K. Temperature dependence of elastic, dielectric, and piezoelectric properties of "single crystalline'' films of vinylidene fluoride trifluoroethylene copolymer. *J. Appl. Phys.* **81**, 2760-2769 (1997).

23. Gomes, J., Serrado Nunes, J., Sencadas, V. & Lanceros-Mendez, S. Influence of the β-phase content and degree of crystallinity on the piezo- and ferroelectric properties of poly(vinylidene fluoride). *Smart Mater. Struct.* **19**, 065010 (2010).

24. Katsouras, I., Asadi, K., Li, M., van Driel, T. B., Kjær, K. S., Zhao, D., Lenz, T., Gu, Y., Blom, P. W. M., Damjanovic, D., Nielsen, M. M. & de Leeuw, D. M. The negative piezoelectric effect of the ferroelectric polymer poly(vinylidene fluoride). *Nat. Mater.* **15**, 78-84 (2016).

25. Liu, Y., Aziguli, H., Zhang, B., Xu, W., Lu, W., Bernholc, J. & Wang, Q. Ferroelectric polymers exhibiting behaviour reminiscent of a morphotropic phase boundary. *Nature* **562**, 96-100 (2018).

26. Huang, Y., Rui, G., Li, Q., Allahyarov, E., Li, R., Fukuto, M., Zhong, G.-J., Xu, J.-Z., Li, Z.-M., Taylor, P. L. & Zhu, L. Enhanced piezoelectricity from highly polarizable oriented amorphous fractions in biaxially oriented poly(vinylidene fluoride) with pure β crystals. *Nat. Commun.* **12**, 675 (2021).

27. Zhu, Z. W., Rui, G. C., Li, Q., Allahyarov, E., Li, R. P., Soulestin, T., Domingues Dos Santos, F., He, H. Z., Taylor, P. L. & Zhu, L. Electrostriction-enhanced giant piezoelectricity via relaxor-like secondary crystals in extended-chain ferroelectric polymers. *Matter* **4**, 3696-3709 (2021).

28. Liu, Y., Zhang, B., Xu, W., Haibibu, A., Han, Z., Lu, W., Bernholc, J. & Wang, Q. Chirality-induced relaxor properties in ferroelectric polymers. *Nat. Mater.* **19**, 1169-1174 (2020).

29. Lin, J. J., Malakooti, M. H. & Sodano, H. A. Thermally stable poly(vinylidene fluoride) for high-performance printable piezoelectric devices. *ACS Appl. Mater. Interfaces* **12**, 21871-21882 (2020).

30. Chen, B., Yuan, M., Ma, R. X., Wang, X. H., Cao, W. & Wang, Z. High performance piezoelectric polymer film with aligned electroactive phase nanofibrils achieved by melt stretching of slightly crosslinked poly (vinylidene fluoride) for sensor applications. *Chem. Eng. J.* **433**, 134475 (2022).

31. Tu, Y. L., Zheng, Y., Guo, S. Y. & Shen, J. B. Switchable piezoelectricity of polyvinylidene fluoride films induced by crystal transition in shape memory process. *ACS Appl. Mater. Interfaces* **14**, 40331-40343 (2022).

32. Taguet, A., Ameduri, B. & Boutevin, B. Crosslinking of vinylidene fluoride-containing fluoropolymers. *Adv. Polym. Sci.* **184**, 127-211 (2005).

33. Soulestin, T., Ladmiral, V., Domingues Dos Santos, F. & Améduri, B. Vinylidene fluoride- and trifluoroethylene-containing fluorinated electroactive copolymers. How does chemistry impact properties? *Prog. Polym. Sci.* **72**, 16-60 (2017).

34. Shin, Y. J., Kang, S. J., Jung, H. J., Park, Y. J., Bae, I., Choi, D. H. & Park, C. Chemically cross-linked thin poly(vinylidene fluoride-co-trifluoroethylene)films for nonvolatile ferroelectric polymer memory. *ACS Appl. Mater. Interfaces* **3**, 582-589 (2011).

35. Lovinger, A. J., Davis, D. D., Cais, R. E. & Kometani, J. M. On the Curie temperature of poly(vinylidene fluoride). *Macromolecules* **19**, 1491-1494 (1986).

36. Farmer, B., Hopfinger, A. & Lando, J. Polymorphism of poly(vinylidene fluoride): Potential energy calculations of the effects of head-to-head units on the chain conformation and packing of poly(vinylidene fluoride). *J. Appl. Phys.* **43**, 4293–4303 (1972).

37. Han, Z. B., Qin, H. C., Chen, X., Xu, W. H., Liu, Y., Bernholc, J. & Wang, Q. Enhanced piezoelectricity in poly(vinylidene fluoride-co-trifluoroethylene-co-chlorotrifluoroethylene) random terpolymers with mixed ferroelectric phases. *Macromolecules* **55**, 2703-2713 (2022).

38. Bargain, F., Thuau, D., Hadziioannou, G., Domingues Dos Santos, F. & Tencé-Girault, S. Phase diagram of poly(VDF-*ter*-TrFE-*ter*-CTFE) copolymers: Relationship between crystalline structure and material properties. *Polymer* **213**, 123203 (2021).

39. Resende, P. M., Isasa, J.-D., Hadziioannou, G. & Fleury, G. Deciphering TrFE fingerprints in P(VDF-TrFE) by raman spectroscopy: Defect quantification and morphotropic phase boundary. *Macromolecules* **56**, 9673-9684 (2023).

40. Li, F., Zhang, S. J., Yang, T. N., Xu, Z., Zhang, N., Liu, G., Wang, J. J., Wang, J. L., Cheng, Z. X., Ye, Z.-G., Luo, J., Shrout, T. R. & Chen, L.-Q. The origin of ultrahigh piezoelectricity in relaxor-ferroelectric solid solution crystals. *Nat. Commun.* **7**, 13807 (2016).

41. Li, F., Lin, D. B., Chen, Z. B., Cheng, Z. X., Wang, J. L., Li, C. C., Xu, Z., Huang, Q. W., Liao, X. Z., Chen, L.-Q., Shrout, T. R. & Zhang, S. J. Ultrahigh piezoelectricity in ferroelectric ceramics by design. *Nat. Mater.* **17**, 349-354 (2018).

42. Frisch, M. J. et al. *Gaussian* (Wallingford CT, 2009).

43. Hariharan, P. C. & Pople, J. A. Accuracy of AH_n equilibrium geometries by single determinant molecular orbital theory. *Mol. Phy.* **27**, 209-214 (1974).

44. Grimme, S., Antony, J., Ehrlich, S. & Krieg, H. A consistent and accurate ab initio parametrization of density functional dispersion correction (DFT-D) for the 94 elements H-Pu. *J. Chem. Phys.* **132**, 154104 (2010).

45. Grimme, S., Ehrlich, S. & Goerigk, L. Effect of the damping function in dispersion corrected density functional theory. *J. Comput. Chem.* **32**, 1456-1465 (2011).

Acknowledgements

This research was supported by the National Natural Science Foundation of China (Grant No. 12274152 and 92366302, Y.L.), the Guangdong Basic and Applied Basic Research Foundation (2024A1515010483, Y.L.), and the initial financial support from HUST (Y.L.). This work is also supported by The Innovative Research Group Project of National Natural Science Foundation of China (High-performance manufacturing of polymer products, 52521002) and Guangdong Provincial Key Laboratory of Manufacturing Equipment Digitization (2023B1212060012). C.Y. Li is supported by the Postdoctor Project of Hubei Province under Grant Number 2025HBBSHCXB095. The authors would thank the Analytical and Testing Center of Huazhong University of Science and Technology for the technical assistance.

Author Contributions

Z.Y. and C.Y.L. contributed equally to this work. Y.L. conceived the idea, designed the research, and supervised the project. Z.Y. synthesized polymer films. Z.Y. collected XRD, XPS and FTIR. Y.L. and Z.Y. performed field-dependent XRD. Z.Y. performed swelling, TGA, DSC and XPS measurements. Z.Y. and Y.T.G. performed electrical, dielectric, and electromechanical measurements. C.Y.L. carried out DFT calculations under supervision by Y.L.. Y.L., Z.Y. and H.M.Z. analyzed the data. Y.L. and H.M.Z. wrote the manuscript with feedback from all authors.

Competing interests

The authors declare no competing interests.

Fig. 1| Crosslinking mechanism in P(VDF-TrFE). a, Sketch of all-*trans* (top) and 3/1-helix (bottom) conformations in ferroelectric polymers. Side view of chain conformation is also provided. The red arrows indicate the projections of the directions of -CF_2- dipole on planes defined by the carbon backbone. The polar direction of all-*trans* and 3/1-helix conformation is denoted by orange arrows. The *gauche* torsional angle τ is also indicated. The structure of PVDF is used to simplify the discussion while the chain tacticity can be introduced by TrFE and CFE based on the above description. **b**, Scheme of crosslinking between P(VDF-TrFE) and ethylenediamine. **c**, FTIR spectra whereas the characteristic absorbance peak of C=N bond at 1652 cm^{-1} is indicated by the dashed line. **d**, XPS spectra (ρ=1.2%) whereas the characteristic peak positions of N-H, C-N, and C=N bonds are indicated by the dashed arrows. **e**, XRD θ-2θ scans. The characteristic peaks of all-*trans* and 3/1-helix conformations are indicated by the star and circle symbols.

Fig. 2| Enhanced d_{33} driven by intermolecular crosslinking. a, Temperature-crosslinking density diagram deduced from dielectric data and DSC results. The grey region is indicative of MPB region. **b**, *P-E* loops measured at 100 Hz. **c**, ΔT_m defined by the frequency-dependent shift in T_m between 1 MHz and 100 Hz. The grey region is indicative of MPB region; Relaxor diffuseness factor γ derived from the dielectric constant at 1 MHz and above T_m. **d**, Enhanced d_{33} by crosslinking. **e**, Electric field induced strain measured at 1 Hz. The linear fit of the data is indicated by the solid line where the slope yields the magnitude of d_{33} through the converse piezoelectric effect. **f**, The d_{33} obtained by different crosslinkers at ρ=1.2%. The error bars in **d** and **f** represent the standard deviation of the mean obtained from at least three measurements using different samples.

Fig. 3| Electric-field-induced phase transition in crosslinked P(VDF-TrFE). a, ρ=0 (Left panel). **b**, ρ=0.3% (Middle panel). **c**, ρ=1.2% (Right panel). The sketch of experimental setup for electric-field-dependent XRD is provided. The characteristic peaks of all-*trans* and 3/1-helix conformations are denoted by the star and circle symbols, respectively. The arrows indicate the trend for increasing the crosslinking density and electric field, respectively.

Fig. 4| The origin of local conformational heterogeneity. a, Sketch of crosslinked helix cured by ethylenediamine after relaxation. **b**, Spatial dependence of local angular distortions $\Delta\tau$ obtained from **a**. The *gauche* angle index is denoted spatially from the left to the right of chains. Specially, the *gauche* angle 1 indicates the first dihedral angle of sequential backbone of C-C-C-C in the left part of the chain. The *gauche* angles 5, 7 and 9 are indicated in **a**. **c**, Energy gain ΔU induced by $\Delta\varphi$ in *gauche* angles 5, 7 and 9 of the top chain in **a**, respectively. **d**, Sketch of crosslinked helix cured by 1,3-diaminopropane after relaxation. The *gauche* angles 5, 7 and 9 are indicated. **e**, Spatial dependence of local angular distortions $\Delta\tau$ obtained from **d**. **f**, Energy gain ΔU with respect to $\Delta\varphi$ in *gauche* angles 5, 7 and 9 of the top chain in **d**, respectively.

Editorial Summary:

The d33 values of ferroelectric polymers are low in comparison to ceramics, such as perovskite oxides. Here, the authors report an intermolecular crosslinking strategy to improve the piezoelectricity of poly(vinylidene fluoride-co-trifluoroethylene) copolymers, achieving high d33 values.

Peer review information: *Nature Communications* thanks the anonymous reviewers for their contribution to the peer review of this work. A peer review file is available.

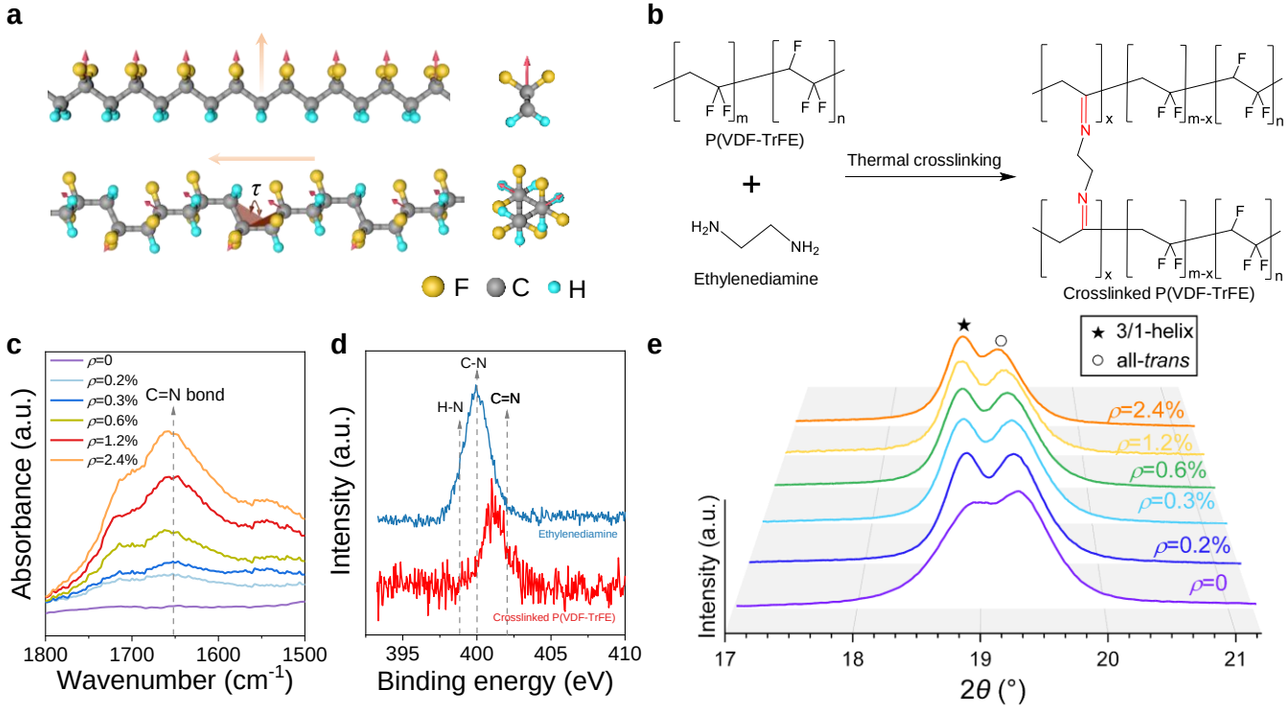
a
F C H
b
P(VDF-TrFE)
Thermal crosslinking
Ethylenediamine
Crosslinked P(VDF-TrFE)
c
ρ=0
ρ=0.2%
ρ=0.3%
ρ=0.6%
ρ=1.2%
ρ=2.4%
C=N bond
Absorbance (a.u.)
Wavenumber (cm-1)
d
C-N
H-N
C=N
Ethylenediamine
Crosslinked P(VDF-TrFE)
Intensity (a.u.)
Binding energy (eV)
e
3/1-helix
all-trans
ρ=2.4%
ρ=1.2%
ρ=0.6%
ρ=0.3%
ρ=0.2%
ρ=0
Intensity (a.u.)
2θ (°)

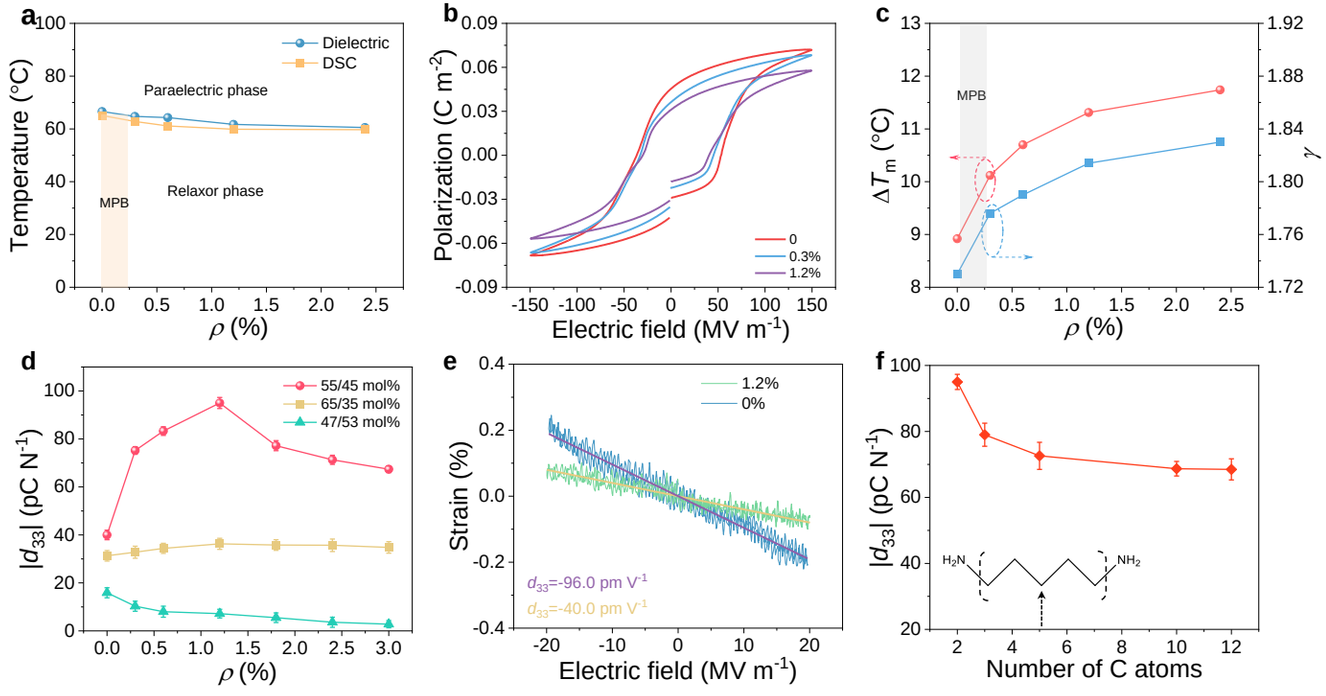
a
Temperature (°C)
ρ (%)
Dielectric
DSC
Paraelectric phase
Relaxor phase
MPB
b
Polarization (C m-2)
Electric field (MV m-1)
0
0.3%
1.2%
c
ΔTm (°C)
γ
ρ (%)
MPB
d
|d33| (pC N-1)
ρ (%)
55/45 mol%
65/35 mol%
47/53 mol%
e
Strain (%)
Electric field (MV m-1)
1.2%
0%
d33=-96.0 pm V-1
d33=-40.0 pm V-1
f
|d33| (pC N-1)
Number of C atoms
H2N
NH2

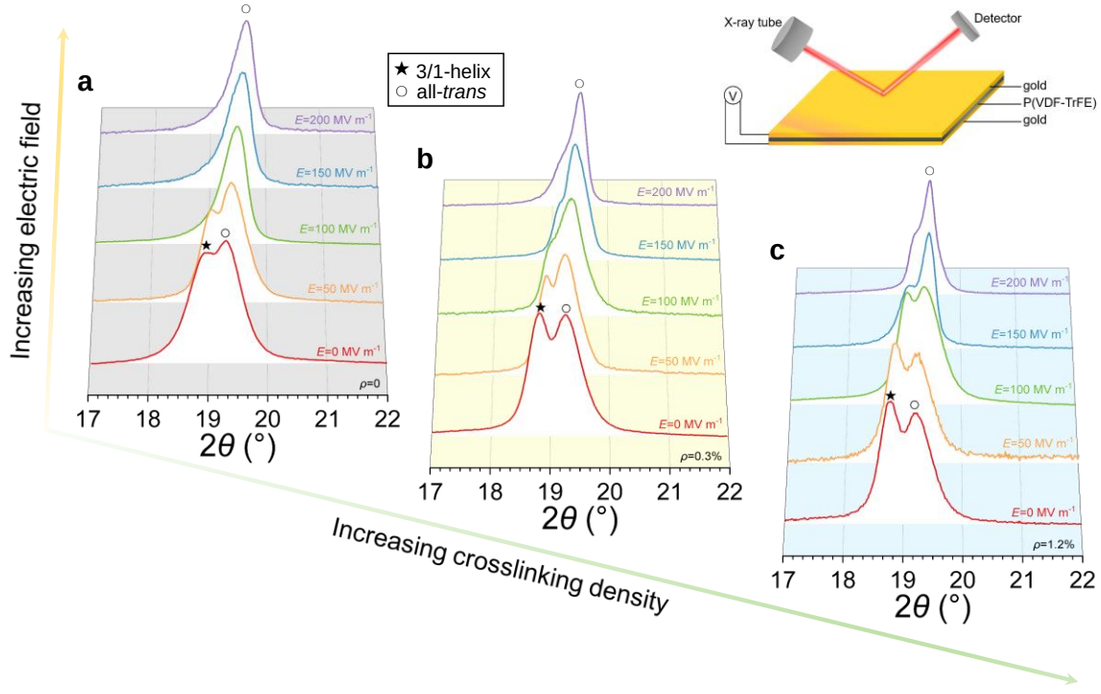
Increasing electric field
Increasing crosslinking density
★ 3/1-helix
○ all-trans
a
b
c
E=200 MV m⁻¹
E=150 MV m⁻¹
E=100 MV m⁻¹
E=50 MV m⁻¹
E=0 MV m⁻¹
ρ=0
ρ=0.3%
ρ=1.2%
17 18 19 20 21 22
2θ (°)
X-ray tube
Detector
V
gold
P(VDF-TrFE)
gold

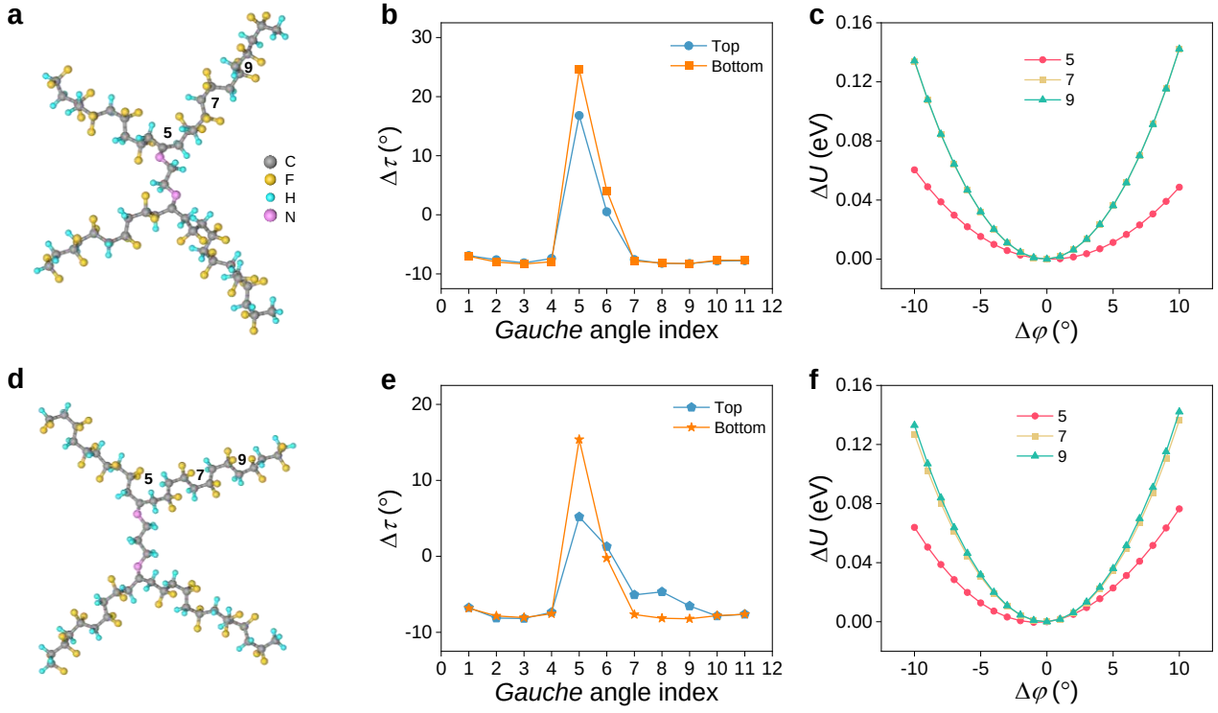
a
9
7
5
C
F
H
N
b
Top
Bottom
Δτ (°)
Gauche angle index
c
5
7
9
ΔU (eV)
Δφ (°)
d
5
7
9
e
Top
Bottom
Δτ (°)
Gauche angle index
f
5
7
9
ΔU (eV)
Δφ (°)